

# Data assimilation for stratified convection

Andreas Svedin<sup>1\*</sup>, Milena C. Cuéllar<sup>2</sup> and Axel Brandenburg<sup>3,4</sup>

<sup>1</sup>*Astronomy Department, Columbia University, New York, NY 10027, USA*

<sup>2</sup>*CUNY - Bronx Community College, 2155 University Avenue Bronx, NY 10453, USA*

<sup>3</sup>*Nordita, KTH Royal Institute of Technology and Stockholm University, Roslagstullsbacken 23, SE-10691 Stockholm, Sweden*

<sup>4</sup>*Department of Astronomy, Stockholm University, SE-10691 Stockholm, Sweden*

26 June 2018

## ABSTRACT

We show how the 3DVAR data assimilation methodology can be used in the astrophysical context of a two-dimensional convection flow. We study the way this variational approach finds best estimates of the current state of the flow from a weighted average of model states and observations. We use numerical simulations to generate synthetic observations of a vertical two-dimensional slice of the outer part of the solar convection zone for varying noise levels and implement 3DVAR when the covariance matrices are scalar. Our simulation results demonstrate the capability of 3DVAR to produce error estimates of system states between up to three orders of magnitude below the original noise level present in the observations. This work exemplifies the importance of applying data assimilation techniques in simulations of the stratified convection.

## 1 INTRODUCTION

When using models to describe the temporal evolution of observed complex systems we are confronted with a number of challenges. An immediate difficulty in dealing with this question is that we generally do not know in all detail the current state of the system or the initial condition that is to be used. Lacking such information prevents us from keeping a model-based simulation in step with the behavior of the observed system.

*Data assimilation* techniques offer means to address such challenges for complex systems by keeping a computer simulation (i.e. model) in synchronization with observations of the system it represents. It provides a general framework for simultaneously comparing, combining, and evaluating observations of physical systems and output from computer simulations. The methods used in data assimilation have been developed over several decades, primarily in meteorology and oceanography for the prediction of the future behavior.

Data assimilation is used daily in operational weather prediction (Bengtsson et al. 1981), in climate forecast (Palmer & Hagedorn 2006) and it was even used to correct the path of the Apollo spacecraft during the first moon landings (Cipra 1993). There is a large and growing body of literature including several monographs (Daley 1993; Kalnay 2003; Wunsch 2006) and work discussing its theoretical foundations (Lorenc 1981; Lorenc 1986; Le Dimet & Talagrand 1986; Ghil 1989). Astrophysical data assimilation has recently been discussed by (Brun 2007), both in the context of space weather and in solar cycle prediction (Dikpati 2007; Choudhuri et al. 2007; Kitiashvili & Kosovichev 2008) as well as in the context of dynamo models (Jouve et al. 2011).

Here we focus on the three-dimensional variational (3DVAR) data assimilation technique, also known as sequential approach (Daley 1993), which produces updates of the current state of a model simulation at times when system observations are available. Propagation of model states between times when the system is observed are free simulations of the model initiated at the latest state estimate. An extension of 3DVAR to implicitly incorporate dynamical information is known as four-dimensional variational (4DVAR) data assimilation. 3DVAR dynamically evolves the mean state whereas 4DVAR also evolves other statistical properties of the model dynamics.

State estimates produced by 3DVAR are optimal provided that the model is linear and the uncertainties are Gaussian. In other words, 3DVAR states are Best Linear Unbiased Estimates, where *best* and *optimal* refer to the lowest possible mean squared error of the estimate (Kalman 1960; Talagrand 1997).

For nonlinear models, error statistics may become non-Gaussian even when the initial distribution is Normal and 3DVAR (or 4DVAR) estimates are not longer unbiased. In this case, data assimilation techniques are challenged by the fact that actual applications are typically based on nonlinear processes (Pires et al. 1996). Specifically, that the states exhibited by real systems under observation will diverge from those predicted by a model simulation is clear and this is principally owing to two causes (Palmer & Hagedorn 2006): observational error and sensitivity to initial conditions. The first of these is a result of what may be called noise. Since its statistical character may not be known, we may need to make some assumptions about its properties. The second source of error occurs on many complex systems and is referred to as chaotic behavior. This has been known for some time, but only in recent decades serious progress in its un-

derstanding has been possible. Sensitivity of the model to initial conditions limits how far into the future predictions can be made (Lorenz 1993).

Among other challenges present for data assimilation of nonlinear model states like the mismatch between spatial locations of observations and grid positions of the model, and the unpaired model variables to observed quantities make the study towards more effective data assimilation techniques an important and demanding area of research. Despite these challenges and open questions, 3DVAR is widely used in the oceanographic and meteorological communities, and would make a good candidate method to be explored in the context of astrophysical flows.

## 2 STRATIFIED CONVECTION MODEL

We are motivated to use data assimilation techniques in the context of stratified convection as a path to obtain predictions of solar subsurface weather events, i.e. the flow structure beneath the surface. Anticipating the possibility of violent events on the solar surface such as coronal mass ejections that affect the space weather and the dynamics of the Earth’s magnetosphere is important, (see Ilonidis et al. 2011). The idea is to use a model of solar subsurface convection, ultimately involving the magnetic fields that give rise to surface activity such as coronal mass ejections, although current attempts in that direction are still at a preliminary stage (Warnecke et al. 2011). However, once such models are able to reproduce sufficient details of solar activity, it will be important to synchronize the model with daily observations to be able to use it for predictions.

As a proof of concept, we design a data assimilation experiment to test the implementation of 3DVAR for the PENCIL CODE, a public domain code of high-order (sixth order in space and third order in time) for solving the hydrodynamic equations (Brandenburg & Dobler 2002)<sup>1</sup>. We consider here a simple two-dimensional convection model representing the turbulent flows of stars with outer convection zones. In our experiment, *synthetic observations* are generated by adding noise to the output from our model. These observations are then processed by 3DVAR to produce an *analysis*. An analysis is an estimation of the *unknown* state of a system in terms of model variables (Lorenz 1986; Talagrand 1997).

Our implementation is general and can in the future be used for other problems that can be addressed with the PENCIL CODE. In this work we assume the model to be *ideal* and reproduces the same features present in the observations. In real world applications, the models are far from ideal, and imperfections and uncertainties related to the model are always present. Ideally, we would like to be able to account for some portion of those unknowns by using data assimilation techniques.

We use the sample `2d/conv-slab-MLT` of the PENCIL CODE (revision r14696 and later). This sample simulates a vertical two-dimensional slice of the outer part of a stellar convection zone. In particular, we use it to simulate convection at low resolution,  $64 \times 64$ , at a Rayleigh number of

$8 \times 10^5$  (Dintrans et al. 2005), and a Reynolds number of approximately 30. The basic setup is similar to that described in (Brandenburg et al. 2005) and other models before them (Hurlburt et al. 1986; Brandenburg et al. 1996), consisting of a convectively unstable layer sandwiched between two stable layers.

The simulated vertical two-dimensional slice of the outer part of the solar convection zone has a mean field velocity of  $u_{\text{rms}} = 0.08$ , the wavenumber of the energy-carrying eddies is  $k_f = 2\pi d$  for a depth of the unstable layer  $d = 1$ , therefore the correlation time  $\tau_{\text{cor}} = (u_{\text{rms}} k_f)^{-1}$  is approximately 2.

Starting from an initial velocity field of perturbations with an amplitude of  $3 \times 10^{-4}$  times the average sound speed, convective motion is generated without having to introduce any stochastic elements. This model is chosen to illustrate 3DVAR in an astrophysical context for its sufficiently complex behavior without having any stochastic elements.

## 3 DATA ASSIMILATION SETUP

The 3DVAR scheme was developed in the meteorological community to improve model-based weather prediction in spite of observational and modeling uncertainties. It was formulated in a unified Bayesian framework by (Lorenz 1986). 3DVAR produces updates of the current state of the system at times when observations are available, which in turn can be used as a new initial condition to be propagated forward to the time when the next observation is available. We can use 3DVAR as a black box along with a low resolution simulation to assimilate many data points at low computational cost on a laptop computer. For example, a typical model run for a  $64 \times 64$  two-dimensional convection field over a time interval of 300 time units takes about 15 minutes on a laptop computer.

3DVAR minimizes the sum of the squared differences between both the model background state and the observations to find a solution that is a compromise between these two estimates of the true state.

It is important to realize that in real problems, the true state is available only through noisy observations of the system. Therefore, it is impossible to tell how close our model output is to current and future true states of the system. In our *twin-experiment* (Bengtsson et al. 1981) we select two different initial fields to run the PENCIL CODE simulation. One of these initial fields represents the unknown true initial state of the system. The other initial field represents what might be, in practice, a good approximation or guess, of the initial state of the system.

As mentioned before, we are set at the ideal case where there is no model uncertainty and the only source of uncertainty is in the observations. In this way, we can assess how far/close the model state is to the true state of the system. The key is to generate a known true state against which the estimated state obtained via data assimilation can be verified.

The experiment is setup as follows: the initial field chosen to represent the true initial state of the system, initializes a model run considered to be the original state of the system to be used as reference trajectory or *control*. The other initial field is used to initialize two different runs: one a *free*

<sup>1</sup> <http://pencil-code.googlecode.com/>

model run and other that will become the assimilated trajectory or *analysis*. The analysis is a collection of segments of model trajectories initialized at the 3DVAR corrections made at all times where the observations are available. The model (analysis) states at the time when an observation is available are known as the *background states*.

Comparison of the free and the control run gives us a measure of the sensitivity to initial conditions of our model, i.e. it shows how similar initial conditions diverge in time.

Similarly, comparing the free run and the analysis represents the effect of the data assimilation procedure over a trajectory starting at the same initial field. If the assimilation of the second set of initial conditions is effective it will bring the analysis “closer” to the control run, and further away from the free run.

We generate synthetic observations by adding independent and identically distributed noise to the horizontal velocity field in all grid-points to the control run. These synthetic data are considered to be our experimental observations which in turn will be used to update the analysis. As is explained in the next section, 3DVAR requires both a model and observation state to find update the analysis at each given time in the assimilation window.

#### 4 3DVAR AND THE WEIGHT FACTOR

The 3DVAR technique finds a model state  $\mathbf{X}$  that agrees with the current state of the system and the information available in the observations and the model. Specifically, we minimize the weighted average of the residues for both observations  $\mathbf{Y}_0$  and model states  $\mathbf{X}_b$  at time  $t$  to find an optimal solution. This is expressed in the 3DVAR cost function (Lorenc 1986)

$$J(\mathbf{X}) = \frac{1}{2} [\mathbf{X} - \mathbf{X}_b]^T \mathbf{B}^{-1} [\mathbf{X} - \mathbf{X}_b] + \frac{1}{2} [\mathbf{Y}_0 - \mathbf{H}(\mathbf{X})]^T \mathbf{R}^{-1} [\mathbf{Y}_0 - \mathbf{H}(\mathbf{X})], \quad (1)$$

where  $\mathbf{X}_b$  is the model state—traditionally called the *background state*,  $\mathbf{Y}_0$  is the observed state,  $\mathbf{B}$  is the background covariance matrix,  $\mathbf{R}$  is the observational covariance matrix, and  $\mathbf{H}$  is the observation operator.

The analysis is  $\mathbf{X}_a$ , minimizes  $J(\mathbf{X})$  and corresponds to the best estimate of the current state of the system. At that time, the model is integrated using as initial condition the analysis up to the next time an observation is available.

Synthetic observations are denoted by  $\mathbf{Y}_0$ , these observations contain noise of amplitude,  $\sigma_R$ , proportional to the maximum amplitude of the full 2D vertical velocity field. For example, a noise level of 1% corresponds to  $\sigma_R = 0.01$  for a normalized field or  $\sigma_R = 6 \times 10^{-3}$  for an unnormalized field.

The selection and construction of the observational and background covariance matrices ( $\mathbf{R}$  y  $\mathbf{B}$ ) is of great interest in data assimilation (Bannister 2008a,b). In our case, the observational noise is not correlated in space, and we neglect spatial correlations between model states, making the off-diagonal components of the  $\mathbf{B}$  and  $\mathbf{R}$  matrices vanish. By doing this, we can set these matrices to be scalars,  $\mathbf{R}_{ij} = \delta_{ij} \sigma_R^2$  and  $\mathbf{B}_{ij} = \delta_{ij} \sigma_B^2$ . Without these spatial correlations 3DVAR generates an analysis that is, in general,

less smooth over the two-dimensional domain. In more sophisticated formulations of equation (1), the form of  $\mathbf{B}$  can also include physical constraints to processes not resolved in the model. Literature in this area is extensive, especially in oceanography and meteorology (Dobricic & Pinardi 2008).

In turn, we set the observation operator to be  $\mathbf{H}_{ij} = \delta_{ij}$ . This means that we assume observations cover all grid-points in the model domain, i.e. the observables and model variables belong to the same space. In other words, system and model are the same. In more realistic implementations of 3DVAR,  $\mathbf{H}$  is typically a computer algorithm that cannot be expressed explicitly as a matrix due to its nonlinear nature (Dobricic & Pinardi 2008). For example the transformation between observables and variable might require the modeling of dynamical processes or making averages.

After these assumptions over the matrices in (1), we can translate the cost function to:

$$J(\mathbf{X}) = w (\mathbf{X} - \mathbf{X}_b)^2 + (\mathbf{X} - \mathbf{Y}_0)^2, \quad (2)$$

where  $w$  is the ratio of the scalar variances corresponding to the observed and background states

$$w = (\sigma_R / \sigma_B)^2. \quad (3)$$

In this setting, to find the state vector  $\mathbf{X}_a$  that minimizes (2), we use POWELL minimization (Press et al. 1992).

The coefficient  $w$  in equation (2) behaves as a weight in the optimization process and will be referred to as the *weight factor*.

Solving  $\nabla J(\mathbf{X}) = \mathbf{0}$  yields

$$w(\mathbf{X} - \mathbf{X}_b) + (\mathbf{X} - \mathbf{Y}_0) = \mathbf{0}, \quad (4)$$

and the optimal state of the model that represents the systems given the current observations, or analysis  $\mathbf{X}_a \equiv \mathbf{X}$ , is given by:

$$\mathbf{X}_a = \frac{1}{w+1} \mathbf{Y}_0 + \frac{w}{w+1} \mathbf{X}_b. \quad (5)$$

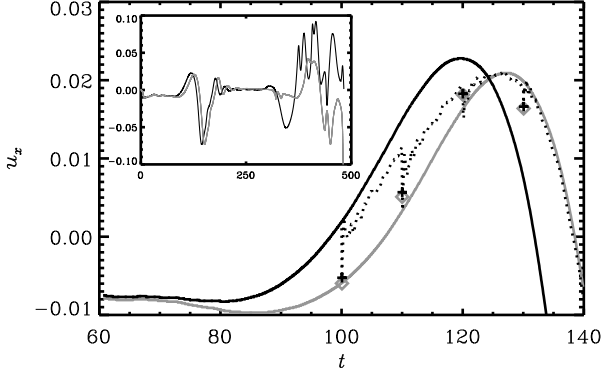
Equation (5) unveils how the contribution of the background states  $\mathbf{X}_b$  and observations  $\mathbf{Y}_0$  affects the analysis  $\mathbf{X}_a$  in terms of the weight factor  $w$ .

Figure 1 clearly shows the result of this process at times where observations (grey  $\diamond$ ) are available, 3DVAR performs a correction given by equation (2) to a value referred to as analysis (black +), and from which a segment of background states (dotted curve) is initialized and run up to the next assimilation time. The analysis is the union of the background states for times different from the assimilation times, and the corrected values obtained at assimilation times.

Given a model and a fixed set of observations, equation (5) help us understand the effects of the weight factor in the resulting analysis  $\mathbf{X}_a$ , as it is detailed in the following paragraphs.

For  $w < 1$  or  $\sigma_R < \sigma_B$ , is interpreted as the case where we assumed that the observational uncertainty is smaller than the model uncertainty, weight is given to the observations since small  $w$  will allow the distance  $(\mathbf{X}_a - \mathbf{X}_b)^2$  to grow without making large contributions to the cost function. In contrast, having a  $w > 1$  will favor model states reflecting our assumption that there is more uncertainty related to the observations than that of the model, or  $\sigma_R > \sigma_B$ .

The next section presents and describes the results of



**Figure 1.** Temporal evolution of the horizontal velocity at a certain midpoint of a 2D convection field for  $t \in [0, 500]$ . Control, free run, and analysis correspond to the grey, black, and dotted curves. A grey ‘ $\diamond$ ’ represent observations, and a ‘+’ corrections ( $\mathbf{X}_a$ ) made by 3DVAR, both at assimilation time.

our numerical experiments. We measure the “quality” of the obtained analyses using 3DVAR by varying values of the weight factor  $w$  as well as a couple of sets of observations with different noise levels.

The correlation time was found to be approximately 2 from simulation parameters (see Section 2). This determine the relevant time scales of the convection features of our simulation and then we choose the most appropriate assimilation time. Consequently, our choice of assimilation time is large enough to let the oscillations propagate over the two-dimensional field but still small enough to be able to capture the smaller scale dynamics. In each 3DVAR experiment, data assimilation corrections are made each 10 time units (sound-travel-time units) and found no fundamental difference when using assimilation times between 5 and 20 time units.

## 5 RESULTS

We generate analyses using 3DVAR for each of the weight factors  $w = \{0, 0.1, 0.5, 1, 10\}$ . For a fixed value of  $w$  we generate an analysis which is the result of assimilating one set of observations with either 1% and 2% noise level for the same set of two initial field conditions.

The resulting horizontal velocity,  $u_x$ , at the midpoint of the upper right quadrant of the two-dimensional domain, is plotted in Figure 2 for  $w = 0$  in the upper panel and  $w = 0.5$  in the lower panel, and in Figure 3 for  $w = 1$  in the upper panel and  $w = 10$  in the lower panel.

Note that grey and dashed lines are the same in all panels since they represent the reference states of the system (control) and the corresponding free run of the model.

Observations are plotted with grey ‘ $\diamond$ ’ symbols. Black ‘+’ marks are used for the corrections calculated at assimilation time by minimizing expression (2). Between assimilations, the analysis is composed by segments of model trajectories (dotted segments) initialized at the corrected state ‘+’ as seen in detail at all insets in Figs. 2 and 3. From equation (5) and these insets, we clearly illustrate the amplitude of the correction made in each case for each value

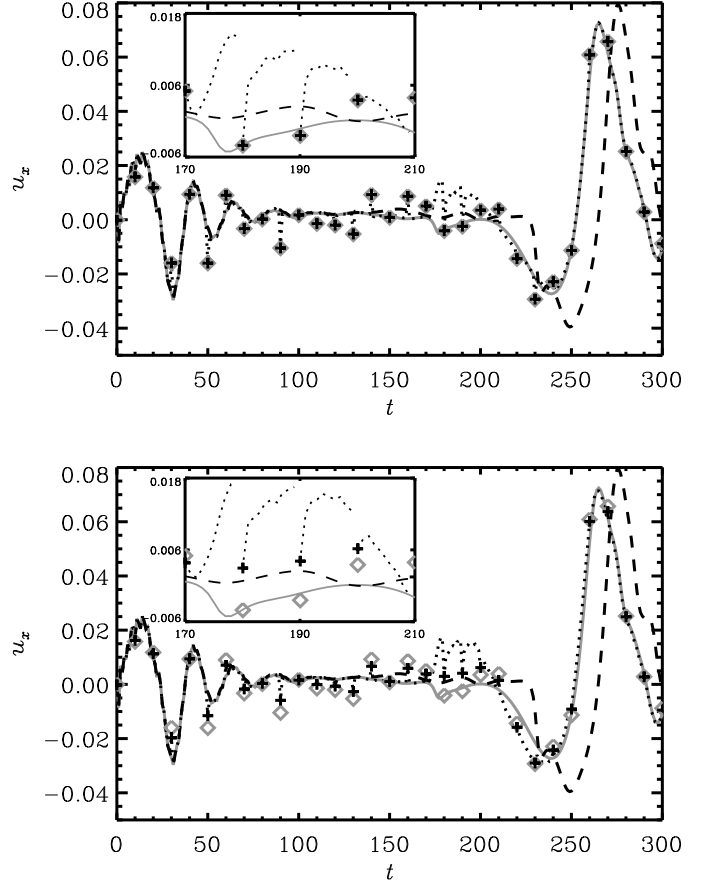


**Figure 2.** Data assimilation run over observations marked with grey ‘ $\diamond$ ’ with 1% noise for  $w = 0$  (upper panel) and  $w = 0.5$  (lower panel). Black ‘+’ marked the 3DVAR correction at assimilation time. Grey, dotted, and dashed curves correspond to the control, analysis, and free trajectories, respectively. Both panels include zoom-ins for  $t \in [170, 210]$ .

of the weight factor  $w$ . This amplitude is measured by the gap between the ‘+’ and the last dot of the previous dotted segment (background states).

For the trivial case of setting  $w = 0$ , the first term in (2) is neglected and the best estimate of the current state of the system is given by  $\mathbf{X}_a = \mathbf{Y}_0$  from in (5), and as seen in the upper panel of Figure 2. The correction (‘+’) is “pulled” from the background state (dotted curve) to the observation (‘ $\diamond$ ’) at assimilation time. The background states are just segments of transient trajectories initialized at the observations.

For any other value of  $w$  the starting point of the correction is in between the observation (‘ $\diamond$ ’) and the end of the previous background states segment (dotted lines); see insets in Figs. 2 and 3.

For  $0 < w < 1$ , the optimal value of the cost-function (2) is by a factor  $1/w$  closer to the observations,  $\mathbf{Y}_0$ , than to the background state  $\mathbf{X}_b$ ; see Eq. (5). The lower panel of Fig. 2 shows results for  $w = 0.5$  where the corrections (‘+’) fall closer to the observations than to the end of the last segment of background states. This figure shows that the analysis follows the control trajectory closely (solid grey

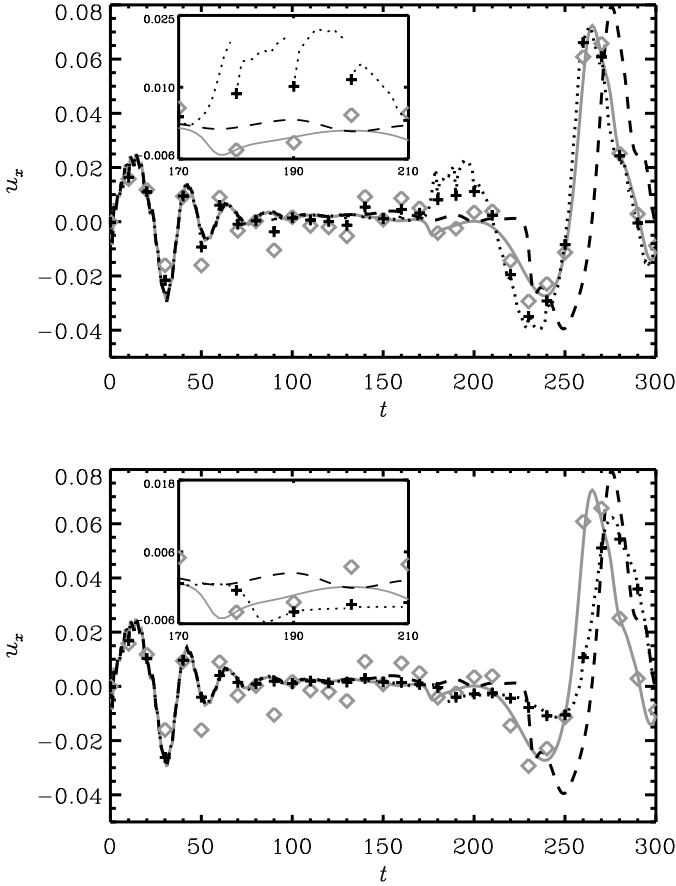


**Figure 3.** Data assimilation run over observations marked with grey ‘o’ with 1% noise for  $w = 1$  (upper panel) and  $w = 10$  (lower panel). Black ‘+’ marked the 3DVAR correction at assimilation time. Grey, dotted, and dashed curves correspond to control, analysis, and free trajectories, respectively. Both panels include zoom-ins for  $t \in [170, 210]$ .

line). Note that even if the corrections are large, e.g. at  $t = 50$  or  $t = 90$ , the analysis quickly relaxes to the control state.

In the case  $w = 1$ , equal weights are given to model states and observations. The optimal value of  $\mathbf{X}_a$  is the average of  $\mathbf{Y}_0$  and  $\mathbf{X}_b$ , from (5). No preference is given to any estimate and the midpoint is the optimal choice for  $\mathbf{X}_a$  as seen in the upper panel of Figure 3.

When  $w > 1$ , the optimization of equation (2) will favor model states rather than observations as follows from equation (5). The analysis at assimilation times is by a factor  $w$  closer to the model states than to the observations. In the lower panel of Fig. 3 we plot the resulting trajectories for this case.

For  $w = 10$ , we observe from this plot and from results at other locations of the two-dimensional domain that for  $w > 1$  the estimates of the original state of the system are biased toward the background states.

When the model is linear and ideal, the analysis produced by 3DVAR will be an unbiased estimate of the true state of the system. There, information about the system is only contained in the experimental observations. When the model is not ideal nor linear, information about the known

unknown processes important to represent the system of interest but not part of the model, could only be included via the  $w$ . In more general terms, through the covariance matrices  $\mathbf{R}$  and  $\mathbf{B}$  which informed the 3DVAR procedure about model and observational known uncertainties.

In this simplified experiment, we can see the great importance of the weight factor  $w$  in 3DVAR. It points out how crucial the construction of the covariance matrices  $\mathbf{B}$  and  $\mathbf{R}$  are for optimal results when using variational approaches of data assimilation. One of the motivations for our choice of  $\mathbf{R}$  and  $\mathbf{B}$  to be scalars is to set a baseline from which we can illustrate, in a simplified way, the inner workings of 3DVAR. It can be hard to see how the different components interact to create a result when more sophisticated choices of  $\mathbf{R}$  and  $\mathbf{B}$  are used.

We would like to note that the zoom-in is chosen to be in the interval  $t \in [170, 190]$ , in all panels of Figs. 2 and 3, as an example of an interval where 3DVAR does not perform very well, and systematically pulls the analysis away from the control trajectory – considered here as the original system trajectory. The reason for this behavior calls for further studies but it is worth noticing that around  $t = 200$  the performance of the assimilation returns to its previous level. The case  $w \geq 10$ , presented in the lower panel of figure 3, actually performs better during this interval.

Consistently, we observe that the analysis is on average closer to the control trajectory than the observations for all values considered for  $w \leq 1$ . As noted, exceptions are observed for larger values of the weight factor and during the interval shown in the insets of Figure 2 and 3.

Tables 1 and 2 present several measures of variation of the output from the simulations of our twin experiment. For each simulation, we calculate the variance of the distances between the control and the observations (Table 1) or the control and the analysis (Table 2) over the data assimilation window.

Specifically, Table 1 shows the variance of the distance between the control trajectory and the free trajectory (first row), and the noisy observations for 1% (second row) and 2% (third row) noise levels at the midpoint of the field (second column) denoted by  $\langle\langle(\delta u_x^0)^2\rangle\rangle$ , this column measures the variability of the local behavior. In addition, the averaged variance over the whole vertical two-dimensional field for the first and the second half of the assimilation window (third and forth column), denoted by  $\langle\langle(\delta^O \mathbf{u}_x)^2\rangle\rangle_T$  where the subscript  $T = 1, 2$  refers to averages over the first or second half of the assimilation window,  $t \in [1, 150]$  or  $t \in [151, 300]$  respectively.

Note that from the values in Table 1, the free run is one or two orders of magnitude further away from the original state of the system (control) than the 1% and 2% noisy observations. Large difference between the second and third columns reflect how free run is diverging from the control run over two different time intervals.

Table 1 is the baseline from which we measure the performance of 3DVAR when estimating the system state from noisy observations or the free trajectory—or 0% noise level—. Note that the variance of the noise is of the order of  $10^{-6}$ . When assessing the performance of 3DVAR for different values of  $w$  and noise levels, we look for variability measures between the control and the analysis lower than the levels set by the free run and the noisy observations.

Noise Level	$\langle(\delta u_x^O)^2\rangle$	$\langle\langle(\delta \mathbf{u}_x^O)^2\rangle\rangle_1$	$\langle\langle(\delta \mathbf{u}_x^O)^2\rangle\rangle_2$
free	1100	530	3000
1%	27	40	36
2%	110	140	140

**Table 1.** Measures of variability (in  $10^{-6}$ ) for the distance between the control and observations with noise levels 1%, 2%, and the free trajectory. See text for notation description.

All variance measures for the free trajectory are larger than the corresponding variances values for all  $w$  and noise levels. This means that performing 3DVAR data assimilation is more effective at estimating the original state of the system than just using as estimate the trajectory initialized with a very close initial field. The variance of the distance between the two initial velocity fields is  $\approx 2 \times 10^{-7}$ .

Table 2 shows the average variance of the distance between control run and the analysis at the midpoint of the field (second column) denoted by  $\langle\langle(\delta u_x^A)^2\rangle\rangle$ , and the averaged variance over the whole vertical two-dimensional field for the first and the second half of the assimilation window (third and forth column), denoted by  $\langle\langle(\delta^A \mathbf{u}_x)^2\rangle\rangle_T$ , for  $T = 1, 2$ , in analogy of the notation used in Table 1.

From the values presented in both tables, we observe that for both noise levels studied and all cases with  $w < 10$ , the variances of the distance between the control and the analysis are smaller—on average—than the corresponding observations with the same noise level. This shows that on both local and global scales, over the two-dimensional domain, 3DVAR is effectively reducing noise and accounting for sensitivity to initial conditions i.e. it is estimating a value for the horizontal velocity closer to the original state of the system (control) than to the trajectory generated using a guess of the initial state of the system (free run).

In contrast, for  $w = 10$  and both noise levels, the free and the analysis are—in average—consistently farther away from the control than the original noisy observations (corresponding values in Table 1) both locally and globally. This is also observed, for example at the specific location of the two-dimensional domain shown in figure 2 and 3.

We note that during the time interval  $t \in [170, 210]$  (see insets of Figs. 2 and 3) this simplified version of 3DVAR under-performs compared to other times. More sophisticated choices for  $\mathbf{R}$  and  $\mathbf{B}$ , that inform more realistically the cost-function (2) about spatial correlations over the field might generate an improved and consistent performance. When comparing in this way the variance of the distance between the control and the free run we write  $\langle\langle(\delta^F \mathbf{u}_x)^2\rangle\rangle_T$ , for  $T = 1, 2$ .

Furthermore, in Figure 4 we plot in a semi-logarithmic scale the variance of the point-by-point distances of the two-dimensional vertical slices between the control and analysis (grey ‘•’), the control and the observations (grey ‘◊’), and the control and the free run (black ‘•’) for all  $t \in [1, 300]$ . The black ‘+’ mark the variance of distances between the control and analysis fields at assimilation times, i.e. when the corrections from (5) are made.

From top to bottom, plots correspond to  $w = 0.1, 1, 10$ . Black dotted and grey ‘◊’ curves are the same for all panel in the figure. The noise level is constant corresponding to 1%.

$w$	$\langle(\delta u_x^A)^2\rangle$	$\langle\langle(\delta \mathbf{u}_x^A)^2\rangle\rangle_1$	$\langle\langle(\delta \mathbf{u}_x^A)^2\rangle\rangle_2$
Noise level 1%			
0	0.61	0.34	3.80
0.1	0.67	0.35	4.40
1	3.30	4.10	<i>130.00</i>
10	<i>300.00</i>	<i>500.00</i>	<i>1600.00</i>
Noise level 2%			
0	2.40	1.30	19.00
0.1	2.70	1.40	22.00
1	33.00	9.80	<i>840.00</i>
10	<i>950.00</i>	<i>430.00</i>	<i>2800.00</i>

**Table 2.** Measures of variability (in  $10^{-6}$ ) for the distance between the control and the analysis for several values of the  $w$  of the  $x$ -component of the velocity,  $\mathbf{u}_x$ . The italic values are larger than the corresponding noise level. See text for notation description.

It is important to note, that values plotted in Figure 4 are not the running variance of the distance between control trajectories and the other relevant trajectories but the variance of the distances between the 2D fields at each time step.

We observe in Fig. 4 that for all values of  $w$  and for  $t \in [0, 10]$  the analysis and free runs are good estimators of the control trajectory. In addition, for all  $w$  and  $t \in [20, 100]$ , the free run and the analysis variances with respect to control, are below the noise level, with the grey curve below the black curve, showing that for 1% noise level 3DVAR produces a better estimate than the free run. Only for  $w = 0.1$  is this the case all values of  $t \in [30, 300]$ . Note the increase in the error of the estimate from  $t \in [160, 190]$ . This is part of the interval shown in the insets for Figs. 2 and 3).

Otherwise, the the error of the estimate exceeds the noise-level for  $t \in [170, 300]$  for  $w = 1$ , and for  $t \in [190, 230]$  for  $w = 10$ .

Figure 4 also shows how far apart—in average—the distance between the control and the free run grows as time increases. The increase in the amplitude of the variance (the black curve) is up to six or seven orders of magnitude over the assimilation window with respect to the same distance at small times. As noted before, this exhibits the model’s sensitivity to initial conditions and it is also a feature observed for all values of the weight factor and noise levels.

In the top panel of the Figure 4, we again see evidence of how the 3DVAR correction (black ‘+’) lands closer to the observations and how the background states start to move towards the control trajectory for lower values of the weight factor,  $w$ . The effect of  $w < 1$  in this case, is to “pull” the background states back closer to the observations as the grey dotted curve is below the corrections (‘+’).

We recall that the weight factor is  $w = (\sigma_R/\sigma_B)^2$ , and it is interpreted here as a measure of the relative confidence given to either the observations and the model. High values of  $w$  reflect higher trust in the observations than in model representation of the system, and the opposite is valid for low values of  $w$ . Note that  $\sigma_B$  relates to initial condition sensitivities than with model deficiencies in our simple setting. As commented earlier, the estimate is sensitive to the choices of  $\sigma_B$  and a more sophisticated choice can include

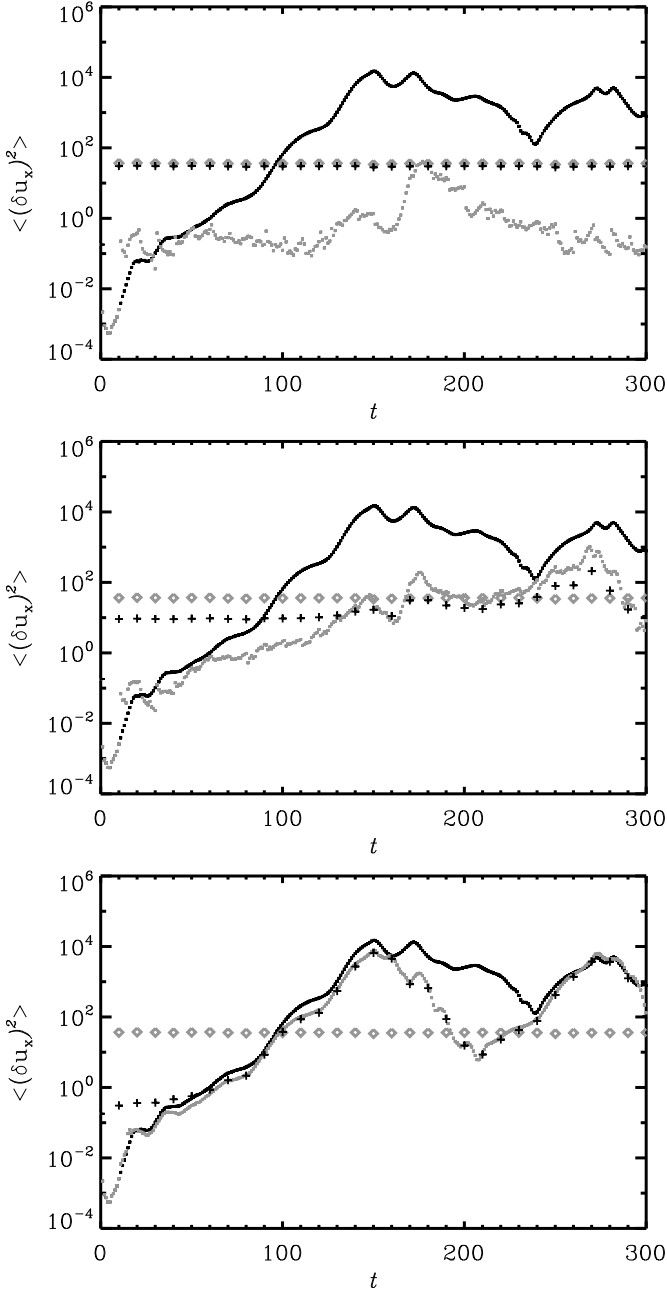


**Figure 4.** Semi-logarithmic plot of the variance of the point-by-point distances of the two-dimensional vertical slices between the control and the analysis in grey ‘•’ ( $\langle (\delta^A \mathbf{u}_x)^2 \rangle$ ), the control and the observations in grey ‘x’ ( $\langle (\delta^O \mathbf{u}_x)^2 \rangle$ ), and the control and the free run in black ‘•’ ( $\langle (\delta^F \mathbf{u}_x)^2 \rangle$ ) for all  $t \in [1, 300]$ . The black ‘+’ corresponds to  $\langle (\delta^A \mathbf{u}_x)^2 \rangle$  at assimilation times, after the correction is made. All quantities are scaled by  $10^6$ .

addition components that might help alleviate some of the model deficiencies.

In conclusion from the results of our experiment, in the particular case where the covariance matrices are assumed to be scalar and for small values of the weight factor  $w$ , the effect of trusting the observations more than the model states ( $\sigma_R < \sigma_B$ ), provides a closer estimate of the original

state of the system than just generating a trajectory close enough in initial conditions. This means that 3DVAR is successful at finding an optimal state estimator in the limit of small observational noise, model uncertainty related only to sensitivity to initial conditions, and scalar covariance matrices,  $\mathbf{R}$  and  $\mathbf{B}$ . Our results strongly point out the importance of choosing more sophisticated covariance matrices ( $\mathbf{R}$  and  $\mathbf{B}$ ) to better inform the assimilation procedure about the known uncertainty sources in a problem of interest.

## 6 DISCUSSION

We have presented an idealized case where model and system are the same: A computer simulation is used both to generate synthetic observations and as the model required for the data assimilation procedure. In this way, we can assess how far/close the model state estimates are to the true state of the system. The key is to have access to the true states that we can use to verify and evaluate estimates obtained using data assimilation.

We used a simplified formulation of the 3DVAR data assimilation technique in terms of the weight factor:  $w = (\sigma_R/\sigma_B)^2$ , that defines the contribution of the model states -that contain propagated information from previous observations- and the current observation to make a state estimate.

This formulation of 3DVAR used here is achieved by reducing the covariance matrices,  $\mathbf{R}$  and  $\mathbf{B}$ , to scalars; and the observation operator,  $\mathbf{H}$ , to the identity. This selection corresponds to neglecting all spatial correlations between model states over the two-dimensional domain in addition to one-to-one correspondence between system observables and model variables. In this way, we clearly separate the contribution of observations and model states to the estimated state, as seen in equation (2) and (5).

It is less direct to see how the different components interact to create an estimate of the original state of the system when more sophisticated choices of covariance matrices, that represent uncertainties and spatial correlations. In that case we would have to think about the optimal combination in analogy to equation (5), in terms of a generalization of the weight factor  $w$  as a *weight matrix*,  $\mathbf{W} = \mathbf{R}\mathbf{B}^{-1}$ . In this analogy, model states and observations will be projected by the matrices  $\mathbf{W}[\mathbf{W} + \mathbb{I}]^{-1}$  and  $[\mathbf{W} + \mathbb{I}]^{-1}$ , respectively, to contribute to the analysis  $\mathbf{X}_a$ . Here,  $\mathbb{I}$  is the identity matrix.

In general, we can say that to understand the 3DVAR algorithm it is important to look at the weight factor, particularly in the limit where  $\mathbf{W}$  is assumed to be the scalar  $w$ .

Consistently we observe that the error between the state estimate and the original state of the system is below the noise level when more weight is given to the observations than to the model state. When the contribution from the model state is larger than the contribution from the observations we note that the error eventually becomes larger than the noise level, see case  $w = 10$ .

We note in Figure 2, 3 and 4 that 3DVAR underperforms for  $t \in [160, 230]$  both locally and globally for all values of  $w$ . Further study of the simulation is needed to account for this atypical behavior.

Minute differences in initial conditions generate differ-

ent time evolution for the different runs, as is expected for nonlinear systems. This is illustrated by the black curves in Figure 4 that present how the variance of the distance between the two initial conditions grows over the time interval. It can also be seen in Figure 1 where the grey and black curves, that started with close initial condition, are very different at latter times.

On the other hand, large correction made by 3DVAR, for example the black '+' at time 50 and 90 in Figure 2, does not appear to have a strong effect. The model run that starts at these far away estimates converges almost instantly back to the control at the same time.

These features, that is reminiscent of chaotic behavior, can be understood in terms of attracting sets where small changes in initial condition generate a different time evolution on the attracting set. A large correction probably takes us outside the attracting set and the solution rapidly falls back when the model is integrated forward.

Another interpretation is that the large correction takes us to states that are not consistent with conservation laws and other physical constraints. The system would then rapidly be forced back onto a more physical state. This dual picture, using both physical and mathematical intuition somewhat clarifies this contradictory behavior.

The 3DVAR methodology is optimal for linear models and Gaussian distributed uncertainties (Lorenz 1986). Very few models in astrophysics have these properties. The validity of variational methods outside the linear or weakly nonlinear case is unclear but if the assimilation is frequent enough the behavior might be closer to linear. Higher assimilation frequency during the interval  $t \in [170, 230]$  might for example give a better result.

The indication of chaotic properties and attracting state space sets invites the use of other data assimilation methods that explicitly take these properties into account (Judd & Smith 2001; Judd et al. 2008). They might be more applicable to non-linear astrophysical processes.

In this work we have used an ideal model, that is, the system and the model is one and the same. There will always be some limitation to modeling of real system and this might prove problematic. In general it is, in our mind, more important for models used for prediction of real systems to be reasonably realistic rather than just being close to the observations.

For nonlinear astrophysical systems that operate on timescales from seconds to years, data assimilation will be of fundamental importance when quantitative agreement between model and observations is to be assessed. The ultimate verification that a model is correct is its ability to make reliable prediction and for this, data assimilation is necessary.

## ACKNOWLEDGEMENTS

We acknowledge the NORDITA data assimilation program of 2011 for providing a stimulating scientific atmosphere. This work was supported by the European Research Council under the AstroDyn Research Project 227952. We also like to thank Professor Spiegel and Dr Dobricic for their help in improving this manuscript.

## REFERENCES

- Bannister R., 2008a, *Quart. J. Roy. Meteor. Soc.*, 134, 1951  
 Bannister R., 2008b, *Quart. J. Roy. Meteor. Soc.*, 134, 1971  
 Bengtsson L., Ghil M., Källén E., 1981, *Dynamic meteorology: data assimilation methods*. Vol. 36, Springer  
 Bengtsson L., Ghil M., Kallen E., eds, 1981, *Dynamica Meteorology: data assimilation methods*. Springer-Verlag  
 Brandenburg A., Chan K. L., Nordlund Å., Stein R. F., 2005, *Astron. Nachr.*, 326, 681  
 Brandenburg A., Dobler W., 2002, *Computer Physics Communications*, 147, 471  
 Brandenburg A., Jennings R. L., Nordlund Å., Rieutord M., Stein R. F., Tuominen I., 1996, *J. Fluid Mech.*, 306, 325  
 Brun A. S., 2007, *Astron. Nachr.*, 328, 329  
 Choudhuri A. R., Chatterjee P., Jiang J., 2007, *Phys. Rev. Lett.*, 98, 131103  
 Cipra B., 1993, *SIAM News*, 26, 757  
 Daley R., 1993, *Atmospheric data analysis*. Cambridge University Press  
 Dikpati M., 2007, *APS Northwest Section Meeting Abstracts*  
 Dintrans B., Brandenburg A., Nordlund Å., Stein R. F., 2005, *A&A*, 438, 365  
 Dobricic S., Pinardi N., 2008, *Ocean Modelling*, 22, 89  
 Ghil M., 1989, *Dynamics of Atmospheres and Oceans*, 13, 171  
 Hurlburt N. E., Toomre J., Massaguer J. M., 1986, *ApJ*, 311, 563  
 Ilonidis S., Zhao J., Kosovichev A., 2011, *Science*, 333, 993  
 Jouve L., Brun A. S., Talagrand O., 2011, *Astrophys. J.*, 735, 31  
 Judd K., Reynolds C., Rosmond T., Smith L., 2008, *J. Atmos. Sci.*, 65, 1749  
 Judd K., Smith L., 2001, *Physica D Nonlinear Phenomena*, 151, 125  
 Kalman R., 1960, *J. Basic Eng.*, 82, 35  
 Kalnay E., 2003, *Atmospheric modeling, data assimilation, and predictability*. Cambridge University Press  
 Kitiashvili I., Kosovichev A., 2008, *Astrophys. J. Lett.*, 688, L49  
 Le Dimet F.-X., Talagrand O., 1986, *Tellus A*, 38, 97  
 Lorenz A., 1986, *Quart. J. Roy. Meteor. Soc.*, 112, 1177  
 Lorenz A. C., 1981, *Monthly Weather Review*, 109, 701  
 Lorenz E. N., 1993, *The essence of chaos*. Seattle: University of Washington Press  
 Palmer T., Hagedorn R., 2006, *Predictability of Weather and Climate*. Cambridge University Press  
 Pires C., Vautard R., Talagrand O., 1996, *Tellus A*, 48, 96  
 Press W. H., Teukolsky S. A., Vetterling W. T., Flannery B. P., 1992, *Numerical recipes in FORTRAN. The art of scientific computing*. Cambridge: University Press  
 Talagrand O., 1997, *J. Meteorol. Soc. Japan*, 75, 191  
 Warnecke J., Brandenburg A., Mitra D., 2011, *A&A*, 534, A11  
 Wunsch C., 2006, *Discrete inverse and state estimation problems: with geophysical fluid applications*. Cambridge University Press